International Journal of Fluid Machinery and Systems
Vol. 2, No. 4, October-December 2009

Original Paper (Invited)

Validation of a CFD model for hydraulic seals

Vincent Le Roy[1], François Guibault[2] and Thi C. Vu[3]

[1]Department of Mechanical Engineering,
[2]Department of Computer Engineering and Software Engineering,
Ecole Polytechnique de Montreal, CP 6079, succ. Centre-Ville, Montreal, QC,
Canada, H3C 3A7, vincent.le-roy@polymtl.ca, francois.guibault@polymtl.ca
[3]Andritz Hydro Ltd., 6100, TransCanadian highway, Pointe-Claire, QC,
Canada, H9R 1B9, thi.vu@andritz-hydro.com

Abstract

Optimization of seal geometries can reduce significantly the energetic losses in a hydraulic seal [1], especially for high head runner turbine. In the optimization process, a reliable prediction of the losses is needed and CFD is often used. This paper presents numerical experiments to determine an adequate CFD model for straight, labyrinth and stepped hydraulic seals used in Francis runners. The computation is performed with a finite volume commercial CFD code with a RANS low Reynolds turbulence model. As numerical computations in small radial clearances of hydraulic seals are not often encountered in the literature, the numerical results are validated with experimental data on straight seals and labyrinth seals. As the validation is satisfactory enough, geometrical optimization of hydraulic seals using CFD will be studied in future works.

Keywords: CFD, SST turbulence model, hydraulic seal, straight seal, labyrinth seal, experimental validation.

1. Introduction

The function of hydraulic seals in Francis turbine runners is to prevent excessive flow leakages. These flow leakages which do not contribute to the turbine power extraction are considered as energy losses. For low head runner turbines, the energy loss due to the flow leakage is not very important, representing about 0.2% of the turbine efficiency. But for high head runner turbines, the seal leakage energy loss could rise to 1% or more of the turbine efficiency. Therefore, hydraulic seals require very small radial clearance to control the flow leakage. But experience has shown that if the radial clearance is less than the radial expansion of the runner, then cold welding could occur during overspeed operation of the runner. The length of the seal contributes also to the control of the seal leakage as the flow rate is reduced with longer seal length. But seals with length longer than necessary will not only cost more but also produce more energy loss due to the seal frictional loss. And seals with too short length will produce cavitation, which rapidly impairs the seal life. In the course of designing a hydraulic turbine, engineers seek to estimate and minimize these losses while respecting all the geometric constraints mentioned above. There are three main types of seals which are widely used and studied in the literature: straight seals, labyrinth seals and stepped seals (or cascade seals) with some variants [2, 3]. Figures 1 to 3 display sketches of these three seal geometry types.

In the sixties and the seventies, experimental investigations for straight and labyrinth seals were carried out in the laboratory of Andritz Hydro Ltd. (formerly Dominion Engineering Works) [4, 5]. These tests results were used to develop semi-empirical solutions for straight and labyrinth seals [6, 7]. The computer programs predict the leakage flow and the frictional loss by application of the turbulent fluid films theory of Elrod and Ng. [8, 9]. The analytical leakage flow was correlated to the experimental results on straight seals, giving a more precise semi-empirical solution. But empirical methods are only successful when applied to seals that are very similar to those which were empirically studied [10]. Nowadays, numerical methods with computational fluid dynamics (CFD) are used to predict seals performance. However most of the numerical studies of seals known to the authors deal with gas labyrinth seals and are performed with k-epsilon turbulence model and wall functions. In the case of hydraulic seals with small radial clearance, the use of low Reynolds turbulence models appears more appropriate. The present study aims to implement an accurate CFD model, using the commercial finite volume CFD code Ansys CFX11, to predict energy losses in hydraulic seals using the SST turbulence model. The experimental data and the semi-empirical programs of Andritz Hydro Ltd. are used for the validation of the numerical results on two types of seals, straight seals and labyrinth seals.

Accepted for publication May 27 2009: Paper number O09045S
Corresponding author: François Guibault, Professor, francois.guibault@polymtl.ca

This manuscript was presented at the 24th IAHR Symposium on Hydraulic Machinery and Systems, October 27-31, 2008, Foz do Iguassu-Brazil.

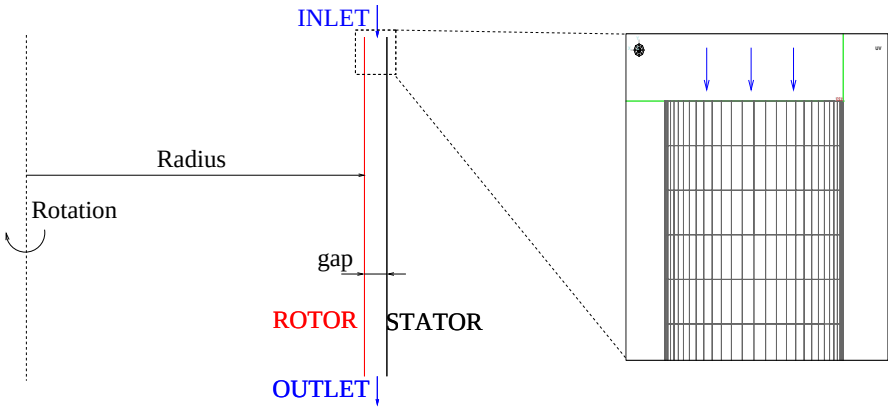

Fig. 1 Straight seal.

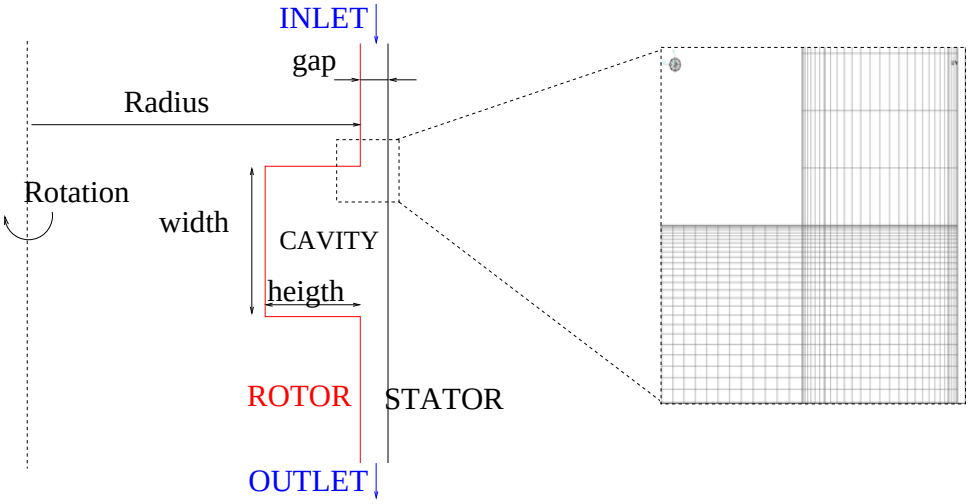

Fig. 2 Labyrinth seal with one cavity.

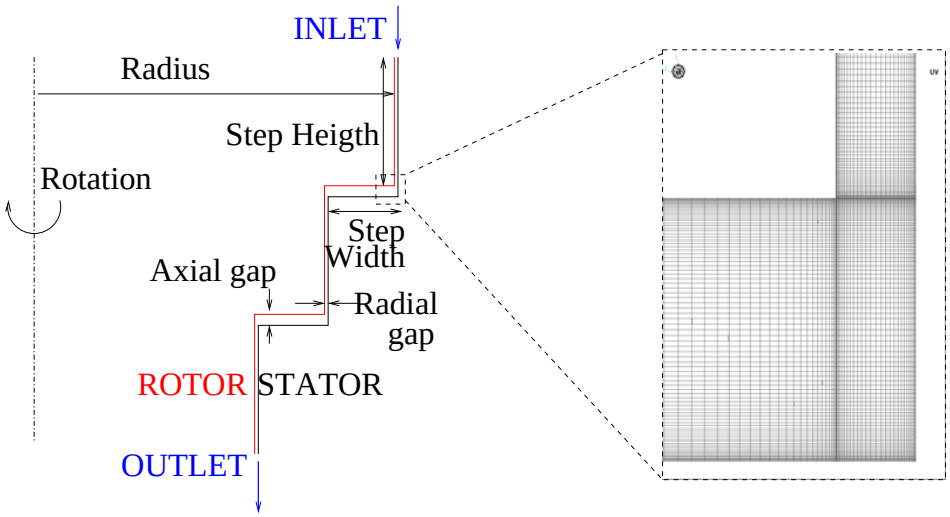

Fig. 3 Stepped seal with two steps.

In this paper we will discuss the following topics:

- Choice of the CFD model for hydraulic seal flow simulation
- Validation of the CFD model on straight seals with experimental data [5] and semi-empirical solutions [7]
- Validation of the CFD model on labyrinth seals with experimental data [6]

The computation results for stepped seals are not presented because no validation with experimental results has been made due to lack of experimental data. Subsequent works to the present study will aim to develop a CFD design tool for seal geometry optimisation (using full Navier-Stokes flow solver and semi-empirical program when available). While some papers have been found in the literature that deal with geometrical optimization of seals, these studies only take into account the leakage loss and deal with labyrinth seals [11, 12]. Our goal is to optimize simpler geometries of straight and stepped seal taking into account both the leakage loss and the frictional loss and combining CFD and a semi-empirical solution to make the optimization process quicker.

2. Choice of the CFD Model

For hydraulic seal simulation, the commercial code Ansys-CFX11 is used in incompressible mode since the fluid is water. The rise of temperature of the water in the seal is small enough to be neglected, as demonstrated in several experimental studies [5, 13]. The problem is isothermal and the physical properties of the fluid are computed using the average temperature of the water in the seal. Since the seal radial clearance is very small compared to the rotor radius, Taylor vortices, source of unsteadiness, are not present in the flow domain. Therefore, only steady state computations are performed.

Fig. 4 (page 403) indicates that the flow is turbulent and Taylor vortices do not appear for most of the cases tested in the straight seal experimental study. Furthermore, Morrisson and al. [13] have shown that the measured turbulence level for labyrinth seals is high. Finally as the flow simulations are for concentric seal geometries, we can consider the problem as axi-symmetric. Since CFX11 does not allow computations in 2D, the computational flow domain consists of a slice of the seal using periodic boundary conditions. Finally the reservoirs upstream and downstream the seal are not modeled to save computational time.

2.1 Low Reynolds SST Turbulence Model

For flow simulation in small radial clearances, a low Reynolds RANS two equations turbulence model without wall functions is required to correctly estimate the viscous dissipation at the walls. Chochua and al. [14] have shown the better performance of a low Reynolds turbulence model over the wall functions model, for the computation of the flow in an annular gas seal with honeycomb walls. In the present study we use the SST turbulence model available from CFX11, which is a mix between a k-omega and a k-epsilon model. When the mesh is fine enough close to the walls ($y+ < 2$) the SST model benefits from the good near-wall behavior of the k-omega model. Typical relative seal surface roughness of the experimental study is about 10^{-3} as the typical radial clearance is about 10^{-3}m and the seal surface roughness is 10^{-6}m. For that reason, we would like to model the surface roughness for the computation but the current implementation of the SST turbulence model in CFX11 does not include the surface roughness treatment.

The numerical result obtained with the SST turbulence model for a concentric smooth surface hydraulic straight seal without rotation has been validated with the analytical result obtained from the Moody diagram. The straight seal of geometry 1 described in Table 2 (page 405) is used for the computation with a flow rate condition corresponding to an axial Reynolds number of 5000. Mesh #1 of Table 1 is used for the computation. The comparison of the predicted flow leakage to the calculation using the Moody diagram gives an error of 2%. With the Moody diagram, one could also estimate the influence of the surface roughness on the flow leakage. Considering a relative surface roughness of 0.001, the rise of the head loss in the seal is estimated to be less than 5% with a maximum experimental axial Reynolds number of 10000 and to be less than 10% with a maximum experimental tangential Reynolds number of 20000.

2.2 Parametric Study of Mesh Characteristics

A structured mesh composed of hexahedrons with only one element in the tangential direction is used. A parabolic mesh distribution in the width of the radial clearance enables us to have small y+ (less than 2) with a reasonable number of points (around 100) to satisfy the requirement of the SST turbulence model. To reduce the total node number, elements are stretched in the flow direction with large aspect ratios, around 200 for the maximum values. Fig. 1 displays a typical mesh at the inlet of a straight seal in the symmetry plane.

The mesh sensitivity is studied using the straight seal of geometry 1 and its operating point described in Table 2 (page 405), with the experimental flow rate corresponding to an axial Reynolds number of 5000. The flow rate is imposed at the inlet and a zero average static pressure is imposed at the outlet. Mesh #1 in Table1 is used as the reference mesh to which numerical result for gradient pressure on other meshes will be compared.

Table 1 Mesh parameters and results of the parametric study of the mesh characteristics on the straight seal geometry 1 described in Table 2.

MESH	h_{min}	Average y+ on the rotor	Distribution	n_{gap}	n_{tng}	max Ax. AR	max Tng. AR	pressure gradient variation
1	0.001mm	y+=1.2	Parabolic	100	1	152	76	2.99E5 Pa
2	0.001mm	y+=1.2	Parabolic	50	1	152	76	1%
3	0.001mm	y+=1.1	Parabolic	200	1	152	76	-0.3%
4	0.003mm	y+=3.4	Parabolic	100	1	51	25	-2.4%
5	0.0005mm	y+=0.6	Parabolic	100	1	205	152	1.7%
6	0.00025mm	y+=0.3	Parabolic	100	1	610	305	2.3%
7	0.001mm	y+=1.2	Parabolic	100	1	20	76	-0.1%
8	0.001mm	y+=1.2	Parabolic	100	5	152	76	0%
9	0.001mm	y+=1.2	Parabolic	100	1	152	152	0.1%
10	0.001mm	y+=1.1	Uniform	100	1	200	150	-4.4%
11	0.001mm	y+=1.2	Uniform	200	1	200	150	-1.5%
12	0.001mm	y+=1.1	Uniform	381	1	200	150	-0.4%

The mesh characteristics used for the parametric study are *type of mesh concentration* (parabolic or uniform), *axial* and *tangential element aspect ratios* (AR), *number of elements in the radial clearance* (n_{gap}) and *in the tangential direction* (n_{tng}), and h_{min}, the *Euclidian distance of the first point to the wall*. The *maximum axial edge length aspect ratio* (max. Ax. AR) is the edge

length in the axial direction over the shortest edge length in the width of the gap. The *maximum tangential edge length aspect ratio* (max. Tng. AR) is the edge length in the tangential direction over the shortest edge length in the width of the gap. With the uniform distribution, the first point next to the wall is set and then the other points are distributed uniformly.

As expected, the influence of n_{tng} (mesh #8) and the influence of the size of the elements edges in the tangential direction (mesh #9) are negligible. The influence of the length of the element edges in the axial direction (mesh #7) is also negligible. Therefore only one element in the tangential direction is needed and a large maximum axial edge length aspect ratio can be used. The leakage loss is more sensitive to h_{min} (meshes #4, #5 and #6) and to n_{gap} (meshes #2, #3). Furthermore the result seems to converge relatively to the mesh when we use more points in the gap. Also, when we use more points in the width of the gap with the uniform distribution (mesh #10, #11 and #12), the result gets closer to the ones obtained with the parabolic distribution: the computation with the uniform mesh #12 gives a result close to the one obtained with mesh #1, composed of almost 4 times less elements.

2.3 Final CFD Model

According to the different numerical tests made, the incompressible, isothermal, stationary, turbulent and axi-symmetric CFD model using the finite volume commercial code Ansys CFX11 is completed with the use of the SST turbulence model and the use of a parabolic mesh in the width of the gap to ensure small y+ (<2) and benefit from the advantages of a low Reynolds turbulence model. The choice of the boundary conditions at the inlet and outlet of the seal, influenced by the test rig geometry, will be discussed in the next section, according to the comparison to experimental data.

As we do not have any information on the turbulence quantities at the inlet of the seal, we use a 10% turbulence intensity at the inlet, which corresponds to the intensity in the developed flow.

3. Validation of the CFD Model with Straight Seal Experimental Data

In the previous section the comparison of the CFD model with the semi-empirical results of the Moody chart for the straight seal without rotation of the rotor is satisfactory. In this section the CFD model is confronted to experimental results on straight seals, with the rotation of the rotor.

3.1 Description of Experiments

The experimental investigation for straight seal (reference [5]) was carried out with various geometric parameters and operating conditions, such as seal radial clearance, from 0.1524mm to 0.762mm (0.006 in to 0.03in), seal length, from 50.8mm to 76.2mm (2 in to 3 in), pressure drop and disk rotational speed (from 0 to 800 RPM). The disk radius is 250 mm. The axial Reynolds number of all test condition varies from 500 to 8000 whereas the tangential Reynolds number varies from 1000 to 34,000. Fig. 4 from DEW internal report [5] (the four flow regions background was found in Kaye and Elgar [15]), shows a map of all operating points tested during the straight seal experimental study. The Taylor number (Ta), in abscissa of the graph, is defined with the Tangential Reynolds (TaR) by: $Ta = TaR\ (gap/radius)^{1/2}$. It clearly indicates that Taylor vortices do not appear for most of the cases. Fig. 5 shows the test rig used for the straight seal experimental investigation. Experimental pressures used as a basis of comparison for our numerical results are measured at the walls of the upstream and downstream reservoirs. Therefore the measured pressure is the total pressure.

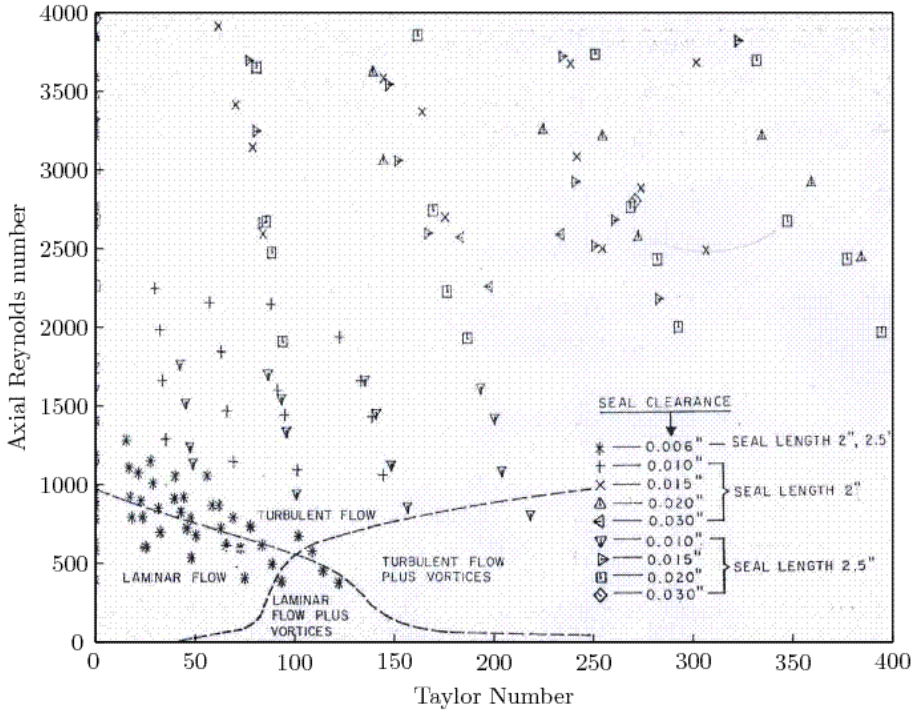

Fig. 4 Distribution of straight seals tests in four flow regions, relatively to Taylor vortices and turbulence.

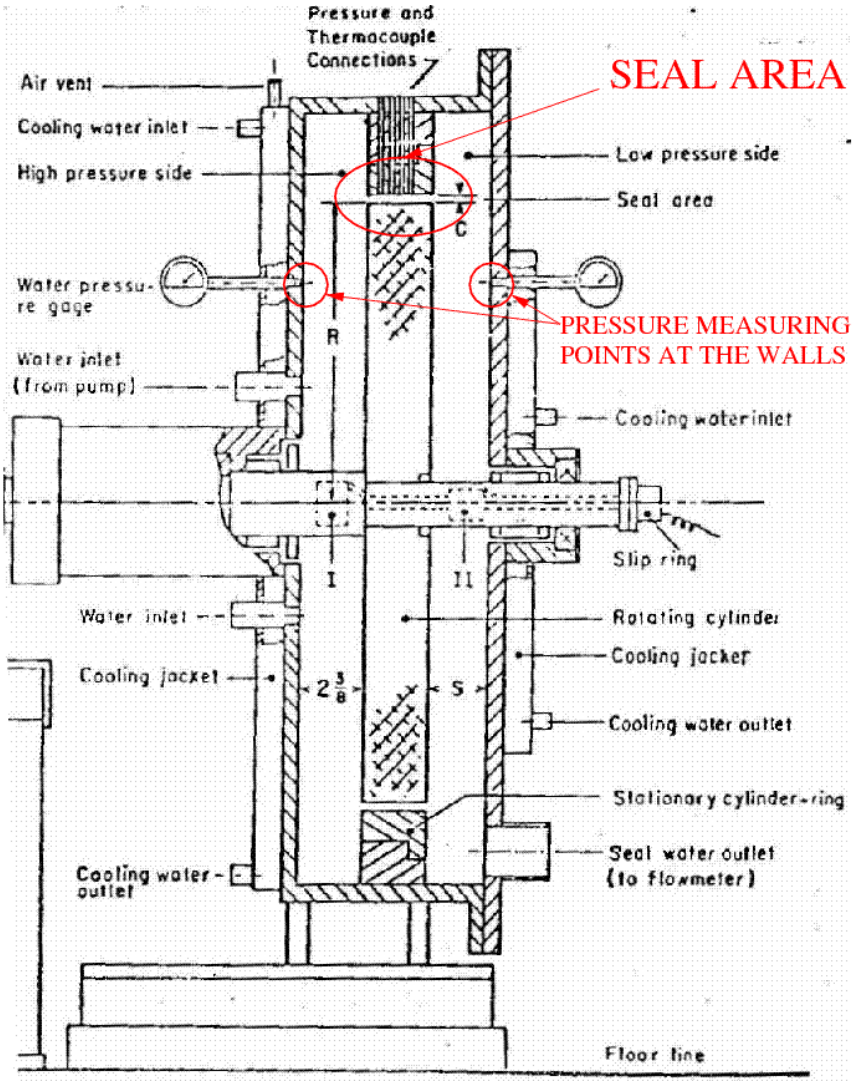

Fig. 5 Test rig used for the straight seal experimental investigation.

3.2 Choice of Boundary Conditions

CFX11 offers different choices of boundary conditions (BC) for inlet, outlet or open faces, on which a flow rate, a total or a static pressure can be imposed. If we impose the flow rate the result of the computation is the pressure gradient. If we impose the pressure gradient the result of the computation is the flow rate.

For **flow rate BC**, the mass flow rate is imposed at the inlet and a zero average static pressure is imposed at the outlet. To compare our numerical results, that do not model the reservoirs, to the laboratory tests, we need to link the pressures at the extremities of the seal to the pressures in the reservoirs. To do so, the kinetic energy losses at the inlet and the outlet of the seal need to be estimated. For an axial duct flow, the common value of the kinetic energy losses at a section change is $k(1/2\rho U^2)$ where U is the mean axial speed and with $k=0.5$ for a sudden contraction and $k=1$ for a sudden expansion. The authors Rhode and al. [10] use these estimates for their static simulation. But, with the rotation of the rotor, the tangential speed of the flow at the outlet is important so that we also estimate the kinetic energy losses at the outlet using the total speed instead of the axial speed in the above formula. These two different kinetic energy losses corrections at the outlet are compared later in this section.

Pressure BC, i.e. imposing the pressures at the extremities of the seal, are more realistic physically. Indeed it is the pressure difference between upstream and downstream regions that imposes the flow in the seal and, before any computation, the pressure gradient is known, unlike the flow rate. So we want to set the values of the pressures at the extremities of the seal while only the pressures in the reservoirs are known (experimental measurements). The kinetic energy losses in the reservoir link the pressure at the extremity of the seal to the pressure in the reservoir. But the kinetic energy losses depend on the unknown mean values of the speed at the inlet and the outlet. However, with the Opening boundary condition type of CFX11, one can set a loss coefficient k with which the imposed pressure is modified with the loss $k\ (1/2)\ \rho\ U_n^2$, U_n being the normal speed on the boundary surface. For pressure BC, the total pressure with a $k=0.5$ loss coefficient is imposed at the inlet and a zero average static pressure is imposed at the outlet, considering the total speed outlet correction for which all the kinetic energy is dissipated in the outlet reservoir.

The convergence of the computation is more difficult with the pressure BC than with the flow rate BC. The use of a loss coefficient at the inlet slows the convergence down as the pressure needs to adjust to the increasing flow rate. Furthermore we note that the monitored average static pressure at the inlet and mass flow rate in the seal are converged only when the maximums

of the residuals of the Navier-Stokes equations reach 10^{-6} (one order of magnitude smaller than for flow rate BC). The use of a bigger time step (up to 4 times the one proposed by CFX11) reduces the number of iterations needed, which is useful for the use of CFD in an optimization process that requires several computations.

3.3 Confrontation to the Experimental Results

We choose 4 different straight seal geometries out of all those tested [5] and several operating points associated for a total of 11 test cases (see Table 2). The range of the gaps is 0.381mm to 0.762mm (0.015in to 0.03in) and the range of the ratio of the tangential Reynolds number over the axial Reynolds number (TaR/AxR ratio) is wide: 1.5 to 5.5. We use mesh #1 in Table 1 for all computations. The resolution of the mesh in the gap is different for each geometry, but introducing more points in the width of the gap does not change significantly the result compared to the errors obtained with the experimental data because the average mesh y+ value always stays below 2.

Table 2 Experimental geometries and operating points of some of the straight seals tested in laboratory.

	Gap	Gap/Radius Ratio	Rotation speed	Nb. of test cases	Axial Reynolds	Taylor number
Geometry 1	0.381mm	0.0015	800 rpm	4	2E3 - 5E3	300
Geometry 2	0.762mm	0.0030	600-800 rpm	5	2.6E3 - 6.4E3	760
Geometry 3	0.508mm	0.0020	800 rpm	1	3.7E3	333
Geometry 4	0.762mm	0.0030	800 rpm	1	6.4E3	962

We compare the discharge coefficients computed with CFD using flow rate BC to experimental data. The discharge coefficient C_d is the ratio of the actual flow rate on the ideal flow rate corresponding to the gradient pressure: $C_d = U/(2\rho H_s)^{1/2}$ with U the average axial velocity and H_s the head loss in the seal. In Fig. 6, the errors in percentage between the numerical and experimental discharge coefficients are displayed, the different test cases being classified with increasing *TaR/AxR* ratios. The numerical discharge coefficients are updated using both the axial and total speed correction for the kinetic energy losses at the outlet. The correction based on the total speed at the outlet gives lower discharge coefficient (higher pressure gradient) than the experimental results. However this correction gives better results for the *TaR/AxR* ratios bigger than 3, for which the axial speed correction at the outlet underestimates the losses at the outlet and gives discharge coefficients that are too large (pressure gradients are too small).

Fig. 7 shows a comparison of the predicted flow discharge and torque, computed with pressure BC, with experimental data and semi-empirical results. The numerical estimate of the kinetic energy losses at the seal outlet is based on the total speed. Figure Fig. 7(left) gives the error in percentage of numerical and semi-empirical values of the discharge coefficient with the experimental results. Numerical and semi-empirical errors are close for *TaR/AxR* ratios bellow 3, but the numerical result is more precise for higher values. As the semi-empirical result for the leakage flow was correlated to many experimental results, it is satisfactory to observe that CFD results stay close to it. The correlation may not have been done for high *TaR/AxR* ratios, for which less experimental tests were made. Fig. 7(right) shows that the numerical values for the friction losses obtained with CFD are closer to experimental values than the semi-empirical values, which were not correlated to experimental data. On the same figure, we observe that the numerical values of the torque exerted on the rotor are bellow the experimental data, which can be explained by the fact that the roughness is not modeled.

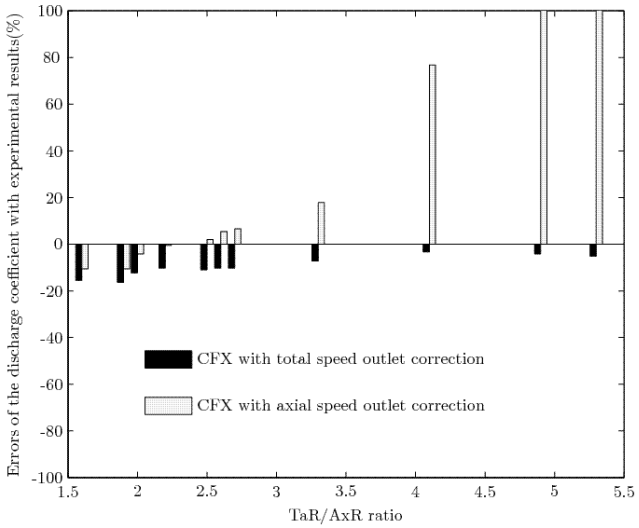

Fig. 6 Comparison of numerical discharge coefficients, computed with the flow rate BC and the 2 corrections, in % of the experimental results.

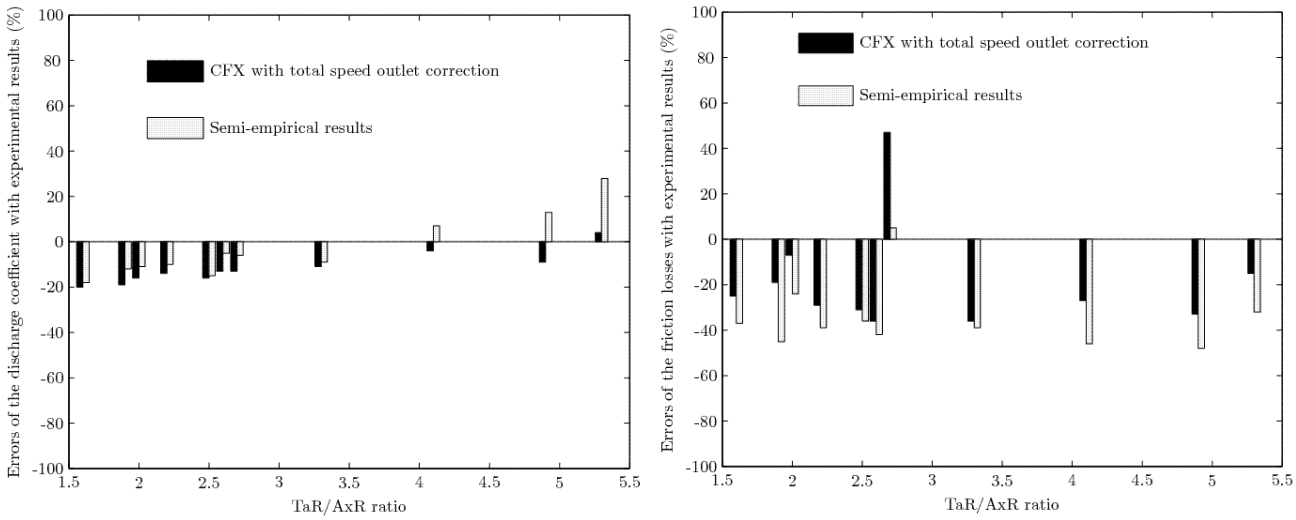

Fig. 7 Comparison of the semi-empirical and the numerical (computed using the pressure BC) discharge coefficients (left) and friction losses (right), in % of the experimental results.

4. Validation of the CFD Model on Labyrinth Seals

Fig. 2 displays a sketch of the geometry of a labyrinth seal with one cavity. The CFD model described in the first section is used and parabolic mesh distributions are used in the width of the gap and in the height and width of the cavity to ensure that the y+ are small enough everywhere. Fig. 2 also displays a detail of the mesh at the entrance of the cavity.

The experimental investigation for labyrinth seals [4, 6] was carried out with various geometric parameters and operating conditions, such as seal radial clearance, from 0.635mm to 2.54mm (0.025 in to 0.1 in), seal length, from 101.6mm to 203.2mm (4 in to 8 in), pressure drop and disk rotational speed (from 0 to 1200 RPM). The disk radius is 230 mm and all the geometries tested only have one cavity. We simulate numerically various operating points on 2 model geometries, with gaps 0.635mm (0.025in) and 2.54mm (0.1in). The experimental and semi-empirical results for the leakage are given as graphs with, in abscissa, the head loss between the reservoirs (in feet$^{1/2}$) and, in ordinate, the discharge coefficient C_d. On the graphs of Fig. 8 and Fig. 9, the black lines are the experimental results and the black dotted lines the semi-empirical results of the computer program. The results are given for 2 rotation speeds: 600rpm and 1200rpm.

The axial speed correction at the outlet does not give good results for small head losses, when the axial speed is low compared to the tangential speed. On the graph of Fig. 8, one can see that the numerical prediction of the leakage, taking into account the total speed correction at the outlet, is not as close to the experimental results as the semi-empirical prediction on geometry 1 with the gap 0.635mm but is closer on geometry 2 with the gap 2.54mm (Fig. 9). The CFD on labyrinth seals is more or less precise (depending on the test case considered) than the semi-empirical program for the prediction of the leakage loss.

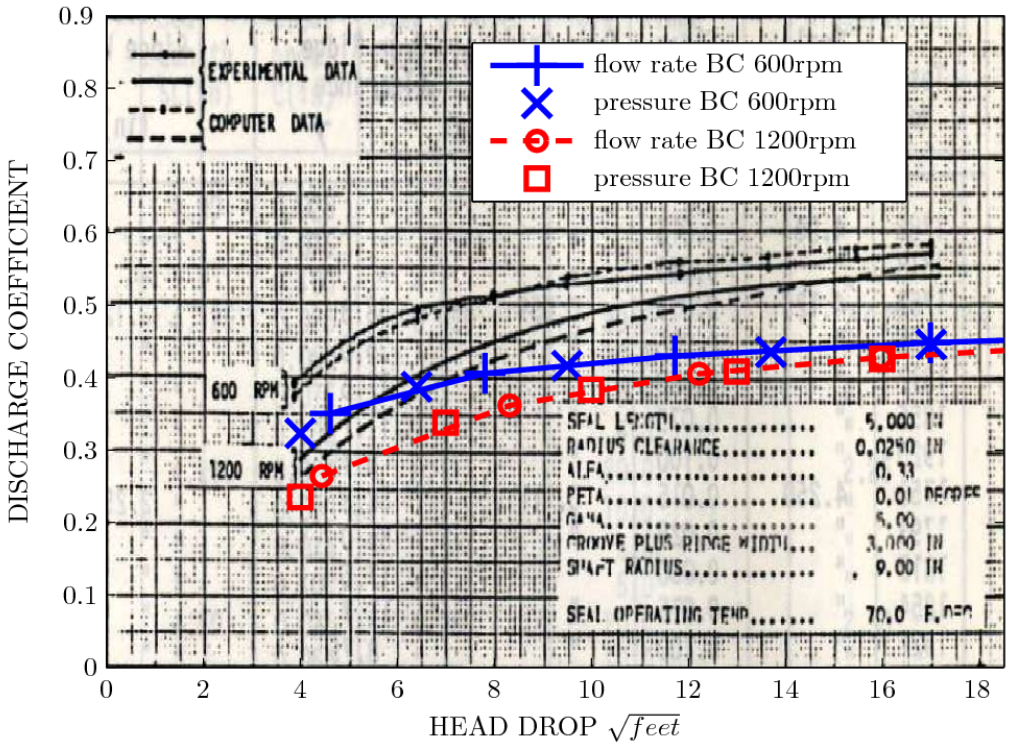

Fig. 8 Numerical results with correction based on the total velocity at the outlet at 600 and 1200 rpm (gap=0.635mm)

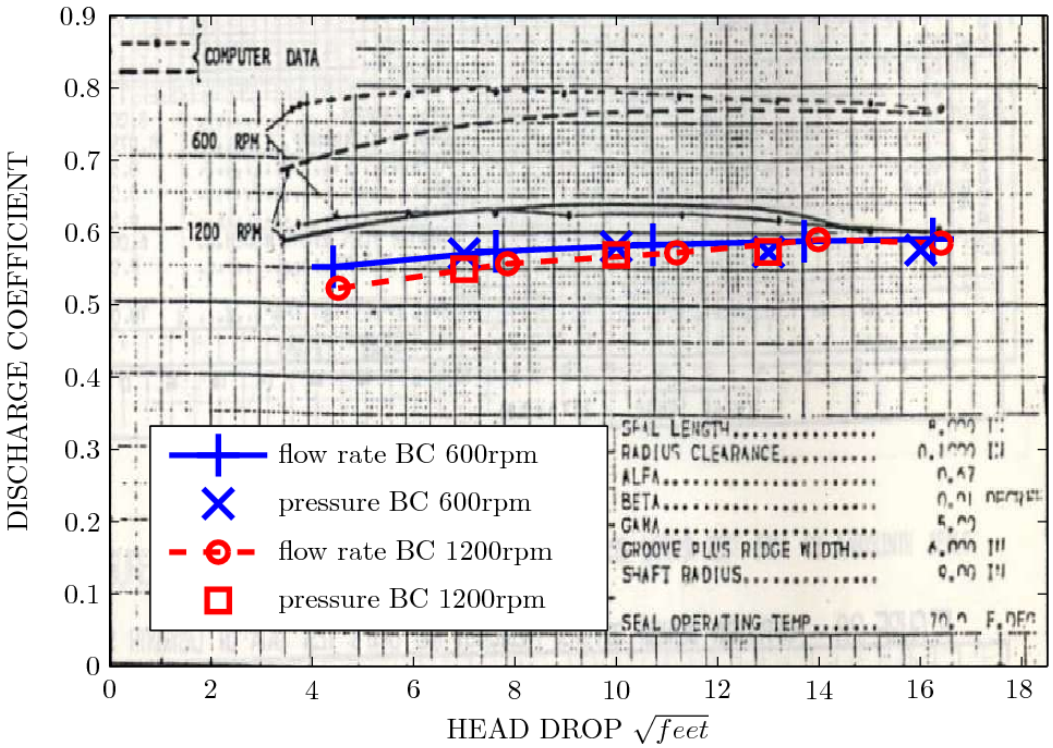

Fig. 9 Numerical results with correction based on the total velocity at the outlet at 600 and 1200 rpm (gap=2.54mm)

We cannot compare the numerical friction losses as we do not have any experimental or semi-empirical results for the torque on labyrinth seals.

5. Conclusion

This paper presents a complete CFD model, using the finite volume commercial CFD code Ansys CFX11, for the computation of the flow in hydraulic seals of Francis runners. This model is incompressible, isothermal, stationary, turbulent with the RANS low Reynolds SST turbulence model, and axi-symmetric. The mesh used is a one layer structured mesh of hexahedrons using parabolic distributions to ensure small y+ at the walls. Numerical tests were made to prove the relevance of the choice of the turbulence model, the mesh and the boundary conditions.

The validation of the CFD model is satisfactory both for straight seals and labyrinth seals. The discrepancies between numerical and experimental results may appear important, the uncertainty on the experimental measurements for the discharge coefficient being 4%, but other factors, like unwanted eccentricity or dynamic behavior, may affect the final experimental results. Furthermore the numerical results for the leakage of a straight seal (related to the discharge coefficient), computed with CFD, are close to the results of the semi-empirical program, which were correlated to many experimental results. Further precision improvements might be obtained through the use of a better estimate of kinetic energy losses in the reservoirs and the inclusion of an adequate roughness model.

The CFD model was also used successfully on stepped seal. Stepped seals are more efficient to reduce leakage than straight or labyrinth seals, owing to the important head loss in the elbows, but manufacturing and assembly costs are more important. The convergence of the computation on a stepped seal is good using parabolic mesh distributions in both the radial and axial gaps, and also in the direction of the flow, allowing an adequately fine mesh at the elbows (see Fig. 3). Unfortunately we do not have experimental results for validation on this more complex flow.

In subsequent works the CFD model proposed and validated in this study will be used for the geometrical optimization of seals to reduce leakage and friction losses. The computations parallelized over several processors (2 to 8) takes between 10 minutes to 1 hour, depending of the geometry. We will try to combine semi-empirical solutions to the CFD model to make the optimization process faster.

Acknowledgments

The authors would like to thank the National Science and Engineering Research Council of Canada (NSERC) for its support of this research, under project CRDPJ 323749-05.

Nomenclature

A_xR	Axial Reynolds number	n_{gap}	Number of elements in the radial clearance
C_d	Discharge coefficient	n_{tng}	Number of elements in the tangential direction
h_{min}	Euclidian distance of the first point to the wall [m]	ρ	Fluid Density
k	Boundary condition blockage factor	Ta	Taylor number
$max\ \ A_x$		TaR	Tangential Reynolds number
AR	Maximum axial element aspect ratio	U	Mean axial velocity [m/s]
max		U_i	Normal fluid velocity at boundary face
$Tng.\ AR$	Maximum tangential element aspect ratio	$y+$	Transformed normal wall distance

References

[1] Rhode, D.L., S.H. Ko, and G.L. Morrison, 1994, "Leakage optimization of labyrinth seals using a Navier-Stokes code," Tribology Transactions, Vol. 37, No. 1, pp. 105-110.

[2] Rhode, D.L., J.W. Johnson, and D.H. Broussard, 1997, "Flow visualization and leakage measurements of stepped labyrinth seals : Part 1-Annular Groove," Journal of Turbomachinery, Vol. 119, No. 4, pp. 839-843.

[3] Rhode, D.L., J.W. Johnson, and D.H. Broussard, 1997, "Flow visualization and leakage measurements of stepped labyrinth seals : Part 2-Sloping Surfaces," Journal of Turbomachinery, Vol. 119, No. 4, pp. 844-848.

[4] Lang, J.H., 1964, "Investigation of discharge coefficient for different labyrinth seal," Dominion Engineering Works, 53-1256BT.

[5] Vu, T., 1976, "Analysis of straight seal tests," Dominion Engineering Works, 1230-7.

[6] Vu, T., 1978, "Viscous seal : theoretical analysis and computer program," Dominion Engineering Works, 1230-18.

[7] Vu, T., 1978, "Straight seal analysis and computer program," Dominion Engineering Works, 1230-17.

[8] Elrod, H.G., 1973, "Some refinements of the theory of the viscous screw pump," ASME Trans. J. Lubric. Technol., Vol. 95, No. 1, pp. 82-93.

[9] Elrod, H.G. and C.W. Ng, 1967, "A Theory of Turbulent Films and its Application to Bearings," ASME J. Lubr. Technol., Vol. 89, No. 1, pp. 347-362.

[10] Rhode, D.L. and G.H. Nail, 1992, "Computation of cavity by cavity flow development in generic labyrinth seals," Journal of Tribology, Vol. 114, No., pp. 47-51.

[11] Asok, S.P., et al., 2007, "Neural network and CFD-based optimization of square cavity and curved cavity static labyrinth seals," Tribology International, Vol. 40, No. 7, pp. 1204-1216.

[12] Schramm, V., et al., 2004, "Shape optimization of a labyrinth seal applying the simulated annealing method," International Journal of Rotating Machinery, Vol. 10, No. 5, pp. 365-371.

[13] Morrison, G.L., M.C. Johnson, and G.B. Tatterson, 1991, "3-D laser anemometer measurements in a labyrinth seal," Journal of Engineering for Gas Turbines and Power, Vol. 113, No. 1, pp. 119-125.

[14] Chochua, G., W. Shyy, and J. Moore, 2002, "Computational modeling for honeycomb stator gas annular seal," Int. J. Heat Mass Transfer, Vol. 45, No. 9, pp. 1849-1963.

[15] Kaye, J. and E.C. Elgar, 1958, "Model of adiabatic and diabatic fluid flow in annulus with an inner rotating cylinder," Transactions of ASME, Vol. 80, No. 1, pp. 753-765.